ADVANCED HEALTHCARE MATERIALS
www.advhealthmat.de

Local and Sustained Baricitinib Delivery to the Skin through Injectable Hydrogels Containing Reversible Thioimidate Adducts

Leo L. Wang, Spencer Tuohy, Karen L. Xu, Arben Nace, Ruifeng Yang, Ying Zheng, Jason A. Burdick, and George Cotsarelis**

Janus kinase (JAK) inhibitors are approved for many dermatologic disorders, but their use is limited by systemic toxicities including serious cardiovascular events and malignancy. To overcome these limitations, injectable hydrogels are engineered for the local and sustained delivery of baricitinib, a representative JAK inhibitor. Hydrogels are formed via disulfide crosslinking of thiolated hyaluronic acid macromers. Dynamic thioimidate bonds are introduced between the thiolated hyaluronic acid and nitrile-containing baricitinib for drug tethering, which is confirmed with ^{1}H and ^{13}C nuclear magnetic resonance (NMR). Release of baricitinib is tunable over six weeks in vitro and active in inhibiting JAK signaling in a cell line containing a luciferase reporter reflecting interferon signaling. For in vivo activity, baricitinib hydrogels or controls are injected intradermally into an imiquimod-induced mouse model of psoriasis. Imiquimod increases epidermal thickness in mice, which is unaffected when treated with baricitinib or hydrogel alone. Treatment with baricitinib hydrogels suppresses the increased epidermal thickness in mice treated with imiquimod, suggesting that the sustained and local release of baricitinib is important for a therapeutic outcome. This study is the first to utilize a thioimidate chemistry to deliver JAK inhibitors to the skin through injectable hydrogels, which has translational potential for treating inflammatory disorders.

1. Introduction

The Janus kinase and signal transducer and activator of transcription (JAK-STAT) pathway has emerged as a disease target for many inflammatory disorders in the skin.[1] To date, several small molecule inhibitors of JAK-STAT signaling have been FDA approved and are highly effective in dermatology, including in atopic dermatitis (e.g., ruxolitinib, abrocitinib, upadacitinib), vitiligo (ruxolitinib), alopecia areata (e.g., ritlecitinib, baricitinib), and psoriasis/psoriatic arthritis (e.g., deucravacitinib, tofacitinib), while many others are currently under investigation for other dermatologic diseases. [2–5] Despite their broad clinical efficacy in dermatology, systemic use of JAK inhibitors is associated with serious risks of infections, major adverse cardiovascular events, thromboses, malignancy, and death leading to a black box warning for all FDA approved JAK inhibitors.[6,7] Due to the risks, medical professionals and patients must exercise caution in their use while patients at high risk for cardiovascular events and malignancy are excluded altogether. As a result, patients are unable to clinically benefit from the effectiveness of these medications without taking on substantial risk.

To overcome limitations of systemic JAK inhibitors, biomaterial-based drug delivery systems can be utilized to retain payloads at the target tissue of interest, maximizing bioavailability while minimizing systemic absorption and off-target toxicities.[8] In this regard, hydrogels are desirable as they are often biocompatible due to their high-water content and they can be engineered to be injectable for minimally invasive delivery.[9] Many hydrogel systems are widely used for the local and sustained delivery of drugs in various medical contexts.[10–13] Thus, we

L. L. Wang, S. Tuohy, A. Nace, R. Yang, Y. Zheng, G. Cotsarelis
Department of Dermatology
Perelman School of Medicine
University of Pennsylvania
1053 Biomedical Research Building, 421 Curie Blvd,
Philadelphia, PA 19104, USA
E-mail: leo.wang@pennmedicine.upenn.edu;
cotsarel@pennmedicine.upenn.edu

S. Tuohy, K. L. Xu, J. A. Burdick
Department of Bioengineering
School of Engineering and Applied Science
University of Pennsylvania
220 South 33rd Street, 107 Towne Building,
Philadelphia, PA 19104-6391, USA

K. L. Xu, J. A. Burdick
BioFrontiers Institute and Department of Chemical and Biological Engineering
College of Engineering and Applied Science
University of Colorado Boulder
1111 Engineering Dr, Boulder, CO 80309, USA

The ORCID identification number(s) for the author(s) of this article can be found under https://doi.org/10.1002/adhm.202303256

DOI: 10.1002/adhm.202303256

sought to engineer an injectable hydrogel to deliver JAK inhibitors to the skin ultimately in the clinic. However, small molecules like JAK inhibitors are challenging to deliver from hydrogels due to their small size and rapid diffusion.[8,14] Previous research delivering JAK inhibitors from hydrogels only showed release over a few days.[15–18] A notable example showed metalloprotease-triggered delivery of tofacitinib for atopic dermatitis in vitro from a polyethylene glycol hydrogel, but with release of ≈40% at 48 h.[19] Despite these illustrations of controlled release, extending release for additional days and even weeks is desired, particularly to avoid the need for repeated administrations where compliance is a major barrier to use and clinical translation.

Recognizing this need, we identified an aliphatic nitrile that is present on numerous clinically approved JAK inhibitors (e.g., baricitinib, ruxolitinib, tofacitinib) that could be used as a reactive electrophile to tether the drug within a hydrogel for controlled and tunable release. Nitriles react with thiols to form thioimidate adducts, which are reversible and dynamic covalent bonds that form through a Pinner-like mechanism between a thiol nucleophile and an electrophilic carbon of a nitrile group.[20–23] The thioimidate represents a transitional state that can be further stabilized through other mechanisms.[24,25] This was first demonstrated through a reversible interaction between benzoylamidoacetonitrile and a cysteine of papain, a papaya cysteine protease; yet, it is now widely accepted that thioimidates form under a range of conditions and also with aliphatic nitriles, where nitrile groups are frequently employed as reversible inhibitors of cysteine proteases (e.g., Cathepsin C inhibitors) by forming thioimidates.[22,23,26,27] Thioimidate bonds are thought to form quickly within 30 min at physiologic conditions (37 °C, pH 7.4) depending on relative electrophilicity. Their reversal can be acid or base-catalyzed, although at physiologic conditions, they exhibit half-lives on the order of seconds to days.[20,28–30] JAK inhibitors in other experimental contexts have been shown to form thioimidate complexes with thiols via nitrile groups.[31] However, the biologic function of the nitrile group in JAK inhibitors is not well understood – in some contexts, they have been shown to reversible engage a thiol (Cys909) in JAK3.[32]

Based on this body of research, we sought to sustain the release of JAK inhibitors from hydrogels that present thiols to form thioimidate bonds with nitriles, leveraging the dynamic and reversible bonds that are needed to bind and then later release drugs in unmodified forms. To this end, we engineered an injectable JAK inhibitor eluting hyaluronic acid hydrogel with a high degree of thiol modification. In this system, thiols on hyaluronic acid are available to (i) bind baricitinib, a representative JAK1/2 inhibitor, and (ii) react with themselves to form disulfide crosslinks to form a hydrogel. We selected the naturally occurring glycosaminoglycan hyaluronic acid for hydrogel formation, as it is biocompatible, widely investigated for drug delivery applications, and commonly used in dermal injectables clinically.[33,34] Using rational design, we investigated the formation of thioimidates with baricitinib, tuned baricitinib release from thiolated hydrogels, and tested our material for JAK-STAT inhibition in vitro and as an injectable therapeutic in vivo in a mouse model of psoriasis.

2. Results and Discussion

2.1. Thioimidate Bond Formation

Previous studies suggest that the nitrile on baricitinib is reactive to thiols and able to form reversible thioimidates through a Pinner-like mechanism (**Figure 1A**).[20] To confirm that baricitinib has a reactive nitrile, cysteamine was mixed with baricitinib at equimolar concentrations for one hour, in concordance of previous reports that the thioimidate forms efficiently at physiologic pH within this time. Using LCMS, we demonstrated resolution of baricitinib (373 Da), cysteamine (77 Da), and the thioimidate adduct of cysteamine and baricitinib (449 Da) eluting with retention times of 0.3, 1.5, and 1.4 s, respectively (Figure 1B). Higher concentrations of baricitinib leading to more product formation are unable to be tested in water due to limitations in solubility; as such, unreacted cysteamine and baricitinib are also present together with their adduct. We similarly observed a product form with baricitinib and L-cysteine (122 Da), yielding an adduct (494 Da) (Figure S1, Supporting Information). We also showed that levamisole (205 Da), a thiazole, does not react with baricitinib to form a product, suggesting that the reactivity with baricitinib is specific to thiol-containing molecules. In the presence of primary amines such as in cysteamine or cysteine, the thioimidate may further be stabilized to form a thiazoline ring; However, the difference in molecular weight is too small between the products to differentiate thioimidate from thiazoline. Importantly, we did not observe a tetrahedral bisadduct that was previously reported to occur with low frequency; this would appear as a product with molecular weight that combines two cysteamines or cysteines and one baricitinib.[35]

Having shown the specificity of baricitinib with thiols, we designed a hydrogel from thiolated hyaluronic acid that directly binds to baricitinib, which also forms disulfide bonds with itself for gel formation. Specifically, thiolated hyaluronic acid formed from the amidation reaction between the carboxyl of hyaluronic acid to cysteamine with a degree of thiol modification of either 30% or 50% and a molecular weight of ≈100 kDa was used (**Figure 2A**).[59] The thiols function to form thioimidates with baricitinib as well as disulfide crosslinks between polymer chains to form hydrogels (Figure 2B).

To test that thiolated hyaluronic acid reacts with baricitinib, we used a commercially available and sensitive fluorogenic substrate that creates a fluorescent product to detect thiols in solution.[36,37] We validated this reagent against a standard dose of glutathione (GSH). In this assay, 10 μM of GSH exhibits an equivalent signal to 10 μM concentration of thiolated hyaluronic acid with 30% modification, consistent with ≈1 thiol per 3.33 disaccharide repeats (**Figure 3A**). Next, baricitinib was titrated into a solution of 25 μM thiolated hyaluronic acid. Increasing concentrations of baricitinib consumed thiols and decreased detection; at equimolar baricitinib nitrile to thiol concentrations, only ≈27% of thiols were consumed on hyaluronic acid (Figure 3B); However, increasing concentrations of baricitinib yielded near complete consumption (≈90%) of free thiols at a molar excess of nitrile of 16 to 1. By assuming equilibrium after one hour, K_{eq} was calculated. In keeping with the dynamic nature of the thioimidate bond, the K_{eq} was highest at a nitrile to thiol ratio of 4 to 1 (Figure 3C). These values likely overestimate thiol consumption by baricitinib given

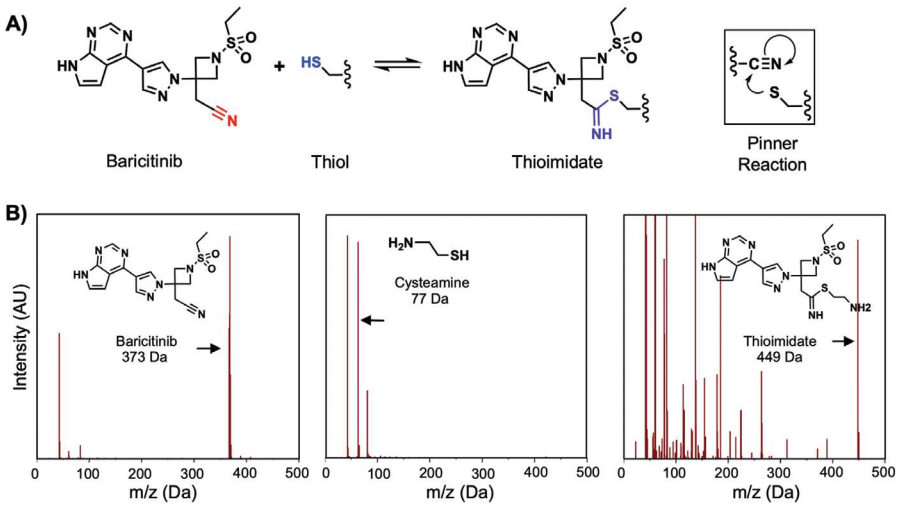

Figure 1. Baricitinib and cysteamine thioimidate formation. A) Baricitinib nitrile (red) interacts with thiols (blue) to form thioimidates (purple). The reaction forms through a modified Pinner reaction in which a free, nucleophilic thiol attacks the electrophilic nitrile on baricitinib. B) Liquid chromatography-mass spectrometry demonstrates product formation between baricitinib (373 Da), cysteamine (77 Da), and baricitinib-cysteamine (449 Da), resolving with three distinct retention time peaks of 0.3 s, 1.5 s, 1.4 s, respectively, which reflect their differences in polarity.

their ability to also form disulfides. Another reactive moiety on hyaluronic acid is the primary alcohol, which may also form imidates with baricitinib, although this reaction is typically acid or base-catalyzed and alcohols are less nucleophilic than thiols.[38] The imidate reaction is likely negligible in the context of these hydrogels.

^{13}C NMR was used to confirm that the formed products between baricitinib and thiolated hyaluronic acid were thioimidates. ^{13}C NMR revealed distinct peaks for both baricitinib and thiolated hyaluronic acid that are consistent with predicted and expected spectra.[23] The ^{13}C NMR spectra of the combined product demonstrated a distinct peak at 170 ppm that was not present in the spectra of the reactants (**Figure** 4A). This is consistent with prior reports for thioimidate carbons as well as the predicted peak from the NMR predict tool at nmrdb.org (Universidad del Valle). Using ^{1}H NMR, we showed that baricitinib has five distinct aromatic protons with peaks between 7–9 ppm. When baricitinib was combined with thiolated hyaluronic acid, the product spectra had a new set of distinct aromatic protons with downfield shifts compared to baricitinib alone, suggesting a second modified baricitinib species was present (Figure 4B). The downfield shift most likely represents a deshielding effect from conjugation of the hyaluronic acid polymer to baricitinib through the thioimidate; in this situation, hyaluronic acid may have electron withdrawing properties. In support of this, four of the five aromatic protons of baricitinib were shifted; the peak at ≈7.7 ppm corresponding to the hydrogen furthest from the thioimidate was not affected, which suggests that the deshielding effect may be related to atomic proximity. Aromatic protons corresponding to the ^{1}H NMR signals are highlighted (Figure S2, Supporting Information).

2.2. Hydrogel Formation and Baricitinib Release

Hydrogels were assembled by mixing baricitinib in solution with thiolated hyaluronic acid (**Figure** 5A). At 2 wt.%, shear oscillatory rheometry was used to confirm formation of a viscoelastic hydrogel where the storage modulus (G′) was higher than the loss modulus (G″) (Figure 5B). Disulfide crosslinks formed over at least 24 h, reaching a final G' of ≈100 and G'' of ≈10 Pa at this timepoint. Moduli were frequency dependent, indicating the dynamic and viscoelastic nature of the material. Moduli were also not affected by temperature. (Figure S3, Supporting Information).[40] No significant differences in moduli were observed between hydrogels without and with baricitinib (Figure 5C). After formation, hydrogels were injectable at 2 and 5 wt.% from 27G x ½″ syringes, requiring ≈2 N and 5 N of force based on force-displacement curves measured by mechanical testing (Figure S4, Supporting Information).

To measure baricitinib release, we determined its absorption properties in the ultraviolet (UV) range, where baricitinib absorbs due to its aromatic ring. Baricitinib absorbed most in the ultraviolet B range (280-320 nm), with absorbance increasing linearly with concentration (**Figure** 6A). This was consistent with prior methods for measuring baricitinib in solution.[40,41] Next, we assembled hydrogels with varying baricitinib loading (0.2 mg mL^{-1}, 2 mg mL^{-1}, corresponding to 40-fold or fourfold thiol excess, respectively), hydrogel concentration (% w/v), and thiol modification (30% or 50%). Baricitinib hydrogels were incubated in PBS at room temperature with releasates collected and replaced regularly over six weeks. At six weeks, hydrogels had nearly fully eroded and were manually disrupted in PBS. Baricitinib in releasates was then quantified by absorbance at 300 nm on a standard curve, where hyaluronic acid is noted to have minimal absorbance.[42–44]

At 0.2 mg mL^{-1} baricitinib, cumulative release profiles of baricitinib were similar for three weeks, regardless of hydrogel concentration or thiol modification (Figure 6B). Specifically, ≈40% was released by one week, 50% by two weeks, and 60% by three weeks; however, by four weeks, differences in release were observed, including 90% release in 2 wt.% 30% mod hydrogels and ≈70% release in 5 wt.% 50% mod hydrogels. In this instance, the latter formulation has four-times the

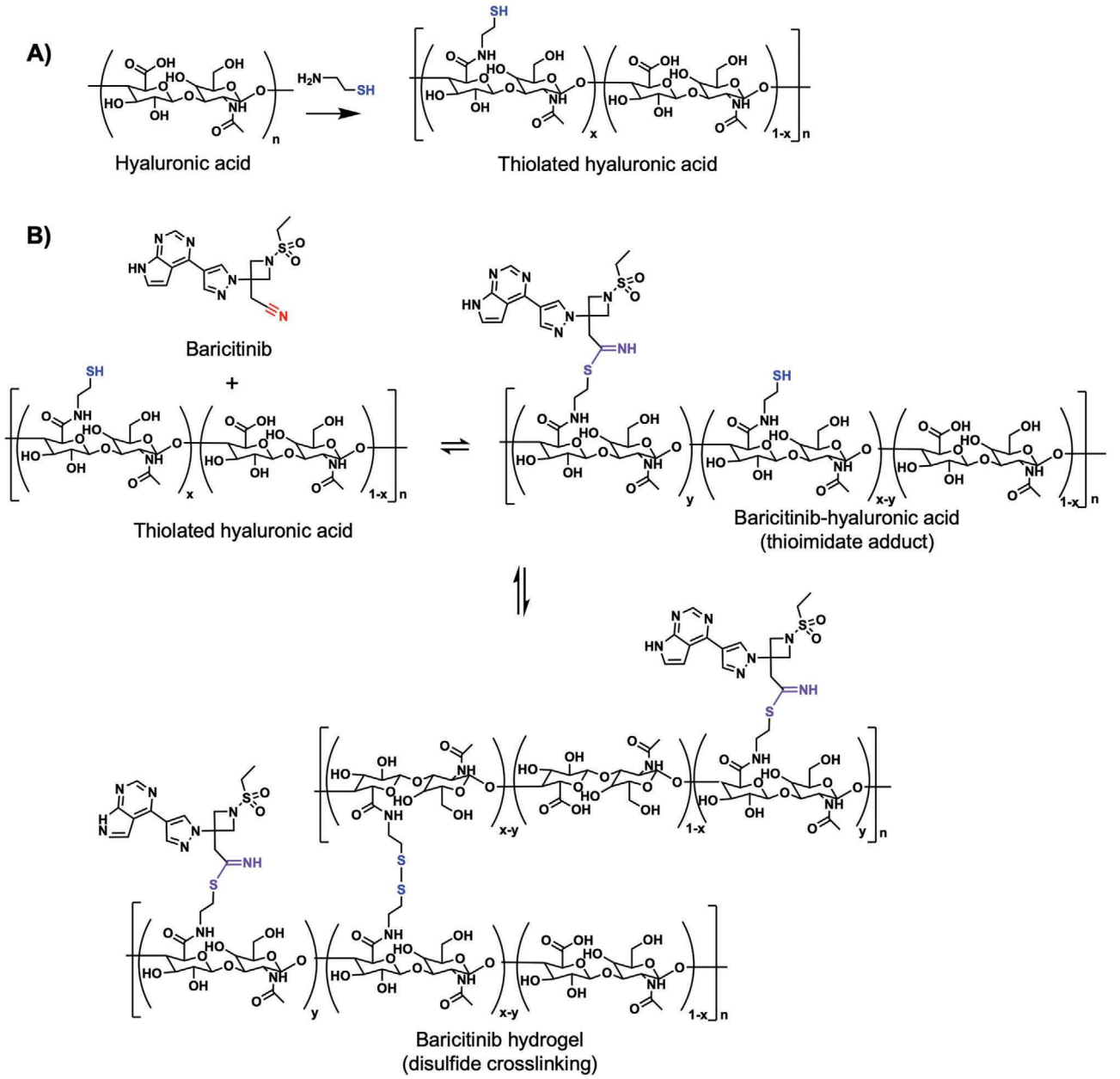

Figure 2. Polymer design, thioimidate bonding, and hydrogel disulfide crosslinking. A) Hyaluronic acid (100 kDa) is amidated at its carboxyl position with cysteamine to yield a thiolated product where x is the fraction of disaccharides with thiol modification and 1-x is the fraction of unmodified disaccharides. B) Baricitinib nitrile (red) interacts with the thiolated hyaluronic acid polymer (blue) to yield thioimidates (purple), where y represents the fraction of disaccharides with bound baricitinib. Simultaneously, unmodified thiols oxidize and form disulfide crosslinks between polymer chains under physiologic conditions to yield a dynamically crosslinked hydrogel. The degree of unbound thiols which form disulfides is represented by x-y and unmodified disaccharides are represented as 1-x.

concentration of thiols, which likely sustains baricitinib release through increased thioimidate formation and increased disulfide crosslinking, thereby decreasing the network mesh size. At 2 mg mL^{-1} baricitinib, there is a larger diffusion gradient due to the higher amount of baricitinib loaded, as well as reduced availability of thiol groups. Consistent with this, release was much faster at this loading with up to ≈70% released by one week, 80% by two weeks, and 90% by four weeks. Significant differences in release were observed before two weeks, where there was faster release in formulations assembled at 2 wt.% compared to formulations assembled at 5 wt.%, consistent with the role of thiols in forming thioimidates and disulfides to slow release. At 2 mg mL^{-1}, baricitinib also began to precipitate over time within the hydrogel, which may also partially contribute to its sustained release. A negligible amount of baricitinib is likely lost during the wash steps and was undetectable at 300 nm. Using the data above, we selected formulations of baricitinib (0.2 and 2 mg mL^{-1}) at 2 wt.% and 30% thiol modification to

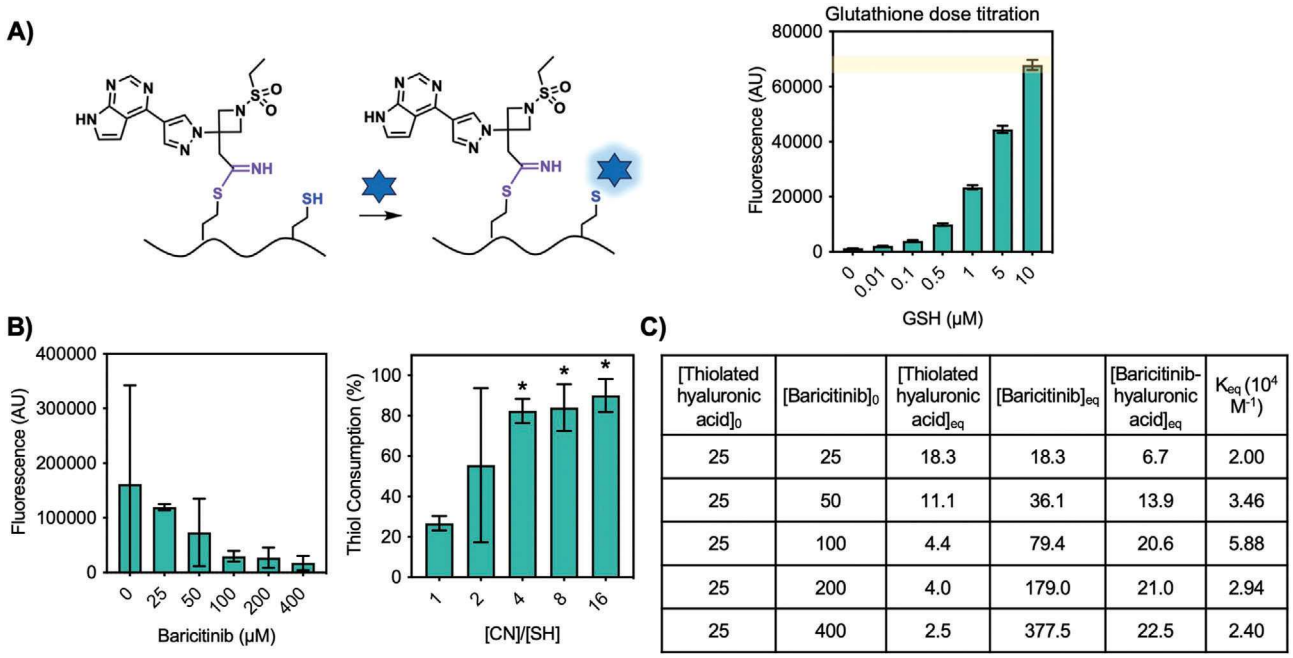

[Thiolated hyaluronic acid]$_0$	[Baricitinib]$_0$	[Thiolated hyaluronic acid]$_{eq}$	[Baricitinib]$_{eq}$	[Baricitinib-hyaluronic acid]$_{eq}$	K_{eq} (10^4 M^{-1})
25	25	18.3	18.3	6.7	2.00
25	50	11.1	36.1	13.9	3.46
25	100	4.4	79.4	20.6	5.88
25	200	4.0	179.0	21.0	2.94
25	400	2.5	377.5	22.5	2.40

Figure 3. Quantification of hyaluronic acid thiolation and consumption of thiols by baricitinib. A) We validated the presence of thiols on hyaluronic acid using a commercially available assay. Fluorescence excitation at 490 and emission at 520 nm was performed using glutathione (GSH) standards and compared to thiolated hyaluronic acid (10 μM, yellow bar), n = 3 per group. B) Thiolated hyaluronic acid (25 μM) was incubated with varying doses of baricitinib (0-400 μM), n = 3 per group. Free thiols were subsequently quantified using the thiol quantification assay demonstrating consumption of free thiols on hyaluronic acid with increasing concentrations of baricitinib. *p<0.05 compared to [CN]/[SH] of 1, n = 3 per group, mean ± SD. Comparison of nitrile to thiol ratio demonstrates incomplete bond formation and reversibility. C) K_{eq} measurements at tested concentrations of [CN]/[SH] of 1, 2, 4, 8, and 16.

test biologic activity (Figure 6C). Of note, while our in vitro data compares relative release between formulations, it may not mimic in vivo conditions, which include hyaluronidases, reducing enzymes, mechanical forces, and other variables.

2.3. In Vitro Activity on JAK-STAT Signaling

To test the effect of released baricitinib in vitro, we used a recombinant HEK293 cell line which contains the firefly luciferase gene stably integrated and under the control of the interferon-stimulated response element.[45,46] In this line, interferon-α (IFNα) binding and activation of JAK1 leads to luciferase expression, enabling rapid and high-through testing of baricitinib activity from hydrogels. We validated this approach by measuring luminescence in response to IFNα stimulation, showing a dose-dependent increase and EC50 of 10.4 U mL^{-1} (**Figure** 7A). After stimulating cells with 100 U mL^{-1} IFNα, we showed that baricitinib decreased luminescence signal with maximal inhibition occurring at 20 μg mL^{-1} (Figure 7B).

For in vitro measurements, we assembled hydrogels at 0.2 or 2 mg mL^{-1} baricitinib at 2 wt.% and 30% thiol modification. Releasates were collected at indicated timepoints and added to HEK293 cultures followed by IFNα stimulation (Figure 7C). To validate differences between baricitinib loading, 5 or 20 μL of releasate was added to cultures (Figure 7D). With 5 μL releasate added, the 0.2 mg mL^{-1} baricitinib formulation led to inhibition only at early timepoints, with diminished activity after three weeks, while the 2 mg mL^{-1} baricitinib formulation led to sustained inhibition at all timepoints. With 20 μL releasate added, near complete inhibition was attained at every timepoint tested from both the 0.2 mg mL^{-1} and 2 mg mL^{-1} baricitinib formulations. Because these conditions demonstrate sustained baricitinib activity in a static environment and with a fixed number of cells, these experiments only allow for comparison between conditions in vitro and are insufficient to suggest in vivo activity. Together, the data suggested that 0.2 mg mL^{-1} baricitinib was sufficient in achieving sustained release and activity in inhibiting JAK-STAT signaling in response to IFNα in vitro. Importantly, no toxicity was observed with addition of releasates to HEK293 cells (Figure S5, Supporting Information). Thus, this formulation (0.2 mg mL^{-1} baricitinib, 2 wt.% hydrogel, 30% thiol modification) was selected for subsequent in vivo studies.

2.4. Hydrogel Injections In Vivo in a Mouse Model of Psoriasis

To test our baricitinib hydrogel for activity in vivo, we utilized a mouse model in which imiquimod, a ligand for Toll-like receptors 7 and 8, is applied daily to dorsal mouse skin to stimulate a psoriasis-like dermatitis characterized by erythema, scaling, and thickening of the epidermis from JAK-STAT signaling.[47,48] Baricitinib has previously been shown to be effective in this mouse model of psoriasis as well as in human psoriasis.[49,50] In this model, the baricitinib hydrogel (0.2 mg mL^{-1} baricitinib, 2 wt.% hydrogel, 30% thiol mod) or controls of PBS, hydrogel,

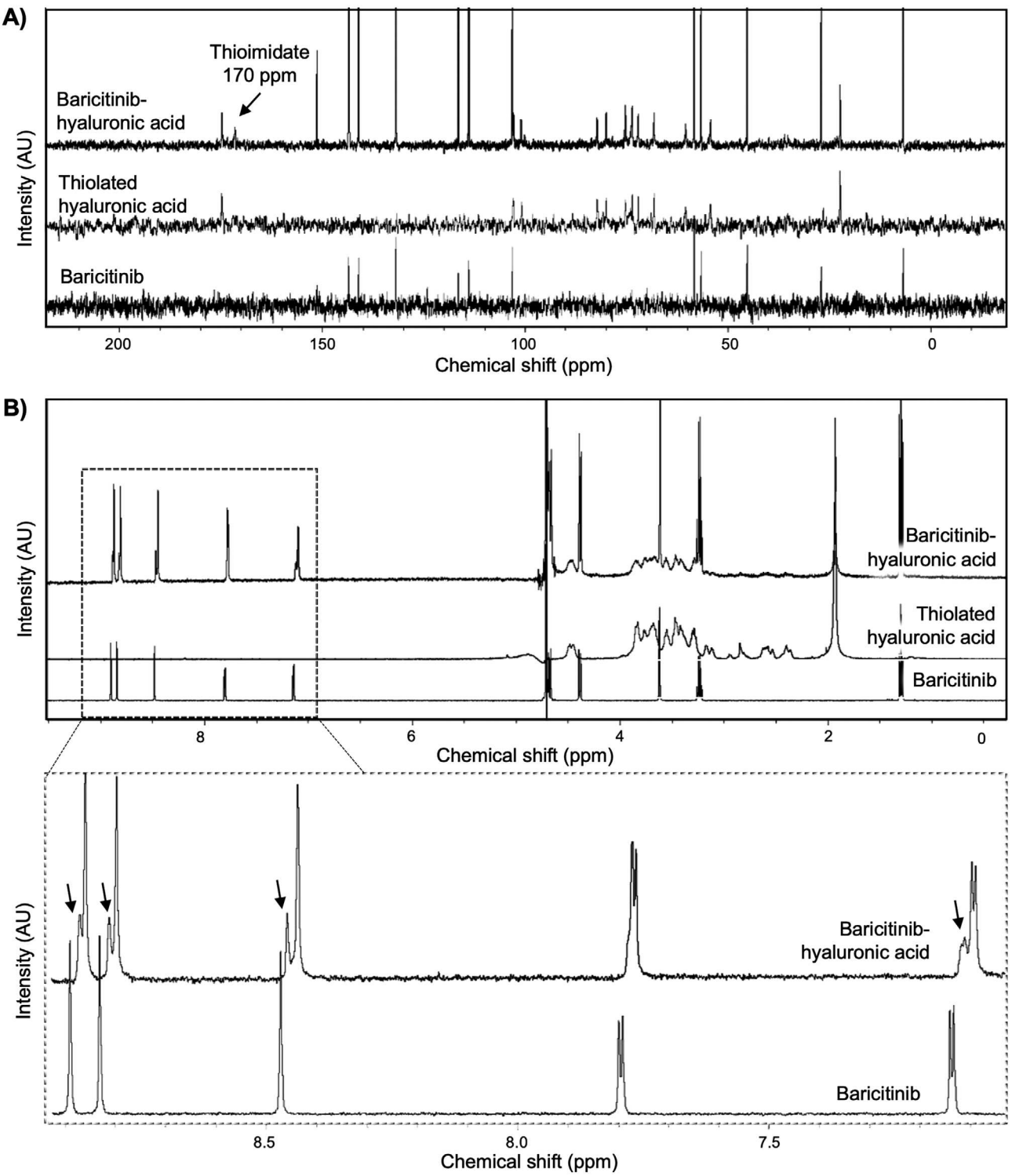

Figure 4. ^{13}C and ^{1}H NMR validate thioimidate formation between baricitinib and thiolated hyaluronic acid. A) ^{13}C NMR of baricitinib, thiolated hyaluronic acid, and the product baricitinib-thiolated hyaluronic acid demonstrate the unique spectra of each individual reactant and a new peak at 170 ppm corresponding to the predicted chemical shift of the thioimidate bond (R-N = C(SR)R). B) ^{1}H NMR of baricitinib, thiolated hyaluronic acid, and the product baricitinib-thiolated hyaluronic acid demonstrate the unique spectra of each individual reactant with distinct aromatic protons in the baricitinib-hyaluronic acid group that is chemically shifted from the aromatic protons of baricitinib alone, suggesting the presence of a modified product in solution consistent with the thioimidate adduct.

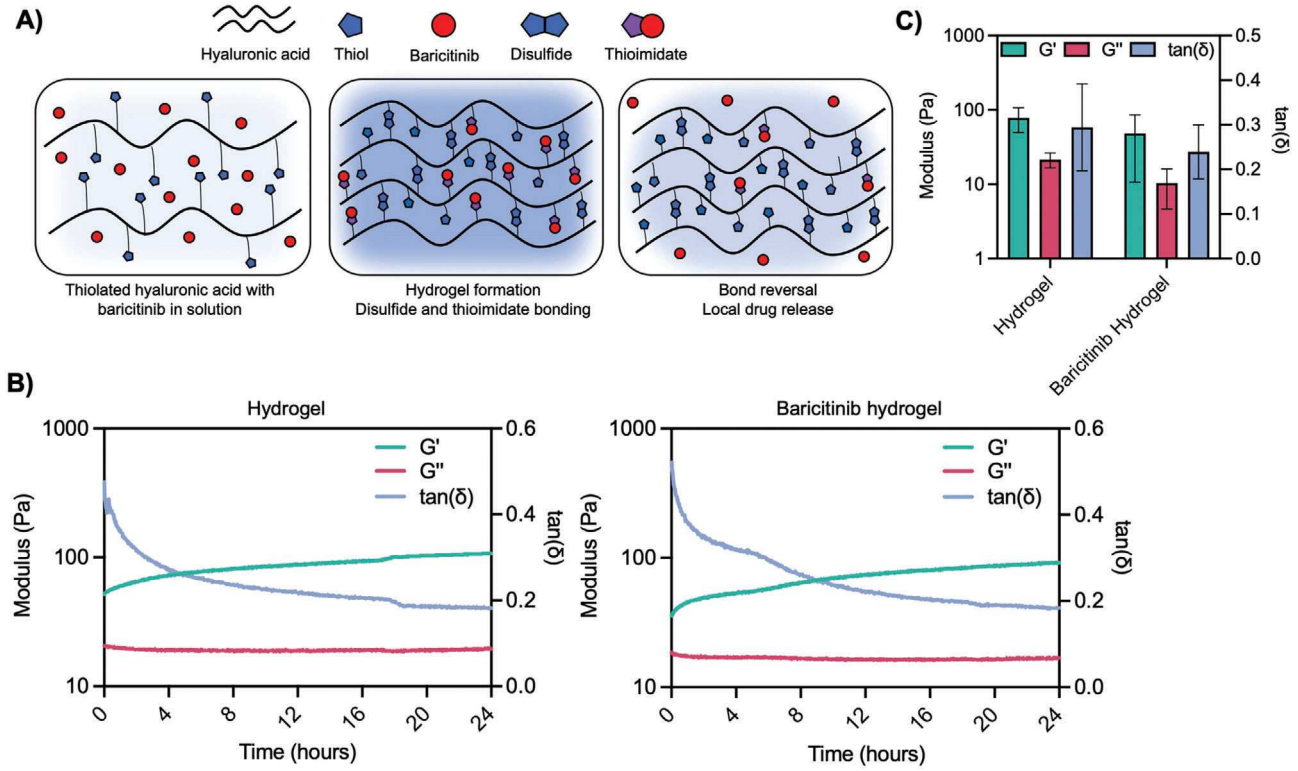

Figure 5. Hydrogel formation and shear oscillatory rheometry. A) Hydrogels are formed between thiolated hyaluronic acid and baricitinib, where thioimidate adducts and disulfide crosslinks form simultaneously. Upon material deposition, thioimidate bonds reverse to release baricitinib into the surrounding environment. B) Shear oscillatory rheometry over 24 h demonstrating crosslinking of polymers into hydrogels (≈100 Pa) with and without baricitinib which occur over the course of 24 h. Frequency sweeps demonstrate classic viscoelastic behavior of materials. C) Mechanical properties of hydrogels and baricitinib hydrogels measured by shear oscillatory rheometry (0.5% strain, 10 Hz) demonstrate comparable properties, n = 3 per group, mean ± SD.

and baricitinib alone were injected (4×25 µL) intradermally into the dorsal mouse skin followed by application of 5% imiquimod cream daily for five days (**Figure** 8A). At seven days, mice were sacrificed, and tissue sections were examined through hematoxylin and eosin (H&E) staining or pSTAT3 immunofluorescence to measure JAK-STAT activity.

Dorsal skin with erythema and scale was present by five days in all groups that were stimulated with imiquimod, which represents psoriasis. Improvements were observed in erythema and scaling in the skin in mice treated with baricitinib hydrogels (Figure 8B). Histologically, imiquimod-stimulated skin exhibited thickened, acanthotic epidermis with parakeratosis, retention of nuclei in the stratum corneum, and pSTAT3 expression in the basal keratinocytes (Figure 8C). Imiquimod led to a fivefold increase in epidermal thickness which was unaffected by treatment with PBS, hydrogel, or baricitinib alone (Figure 8D); However, treatment with baricitinib hydrogels led to reduced epidermal thickness that was not statistically different from epidermal thickness of control skin that did not receive imiquimod. Representative H&E of skin demonstrates consistency in these trends across the entire sectioned epidermis (Figures S6 and S7, Supporting Information). Imiquimod-stimulated skin exhibited increased pSTAT3 nuclear expression in basal keratinocytes which was unaffected by treatment with PBS, hydrogel, or baricitinib alone. However, mice treated with baricitinib hydrogels exhibited decreased pSTAT3 expression (Figure 8C), corroborating the changes in epidermal thickness observed. Weight loss of up to 15% was observed in all imiquimod stimulated groups, with a trend toward improvement in baricitinib hydrogel groups (Figure S8, Supporting Information).

Notably, injected baricitinib alone had no effect, indicating the need for the hydrogel for local retention and sustained release. Further, the benefit seen from the hydrogel indicates the biologic effect is from local rather than systemic activity. We did not observe the hydrogel in all H&E sections, consistent with prior reports that soft, hyaluronic acid-based hydrogels are lost during the processing steps;[39] However, few sections demonstrate hydrogel in the dermis-subcutaneous space junction (Figure S9, Supporting Information).[39,51] Because topical imiquimod is unable to be applied for longer times due to risk for systemic absorption and effects, we are unable to test the efficacy of the hydrogel at later timepoints using this model. Prior reports using similar thiolated hyaluronic acid hydrogels in vivo suggest hydrogels are persistent for several weeks in the skin, during which they may be biologically active.[52–55] Further, clinical evidence from the use of hyaluronic acid hydrogels as cosmetic dermal fillers suggest they are persistent for months to years in the skin.[56,57] Thus, sustained baricitinib activity from our hydrogels is likely to be observed in future studies.

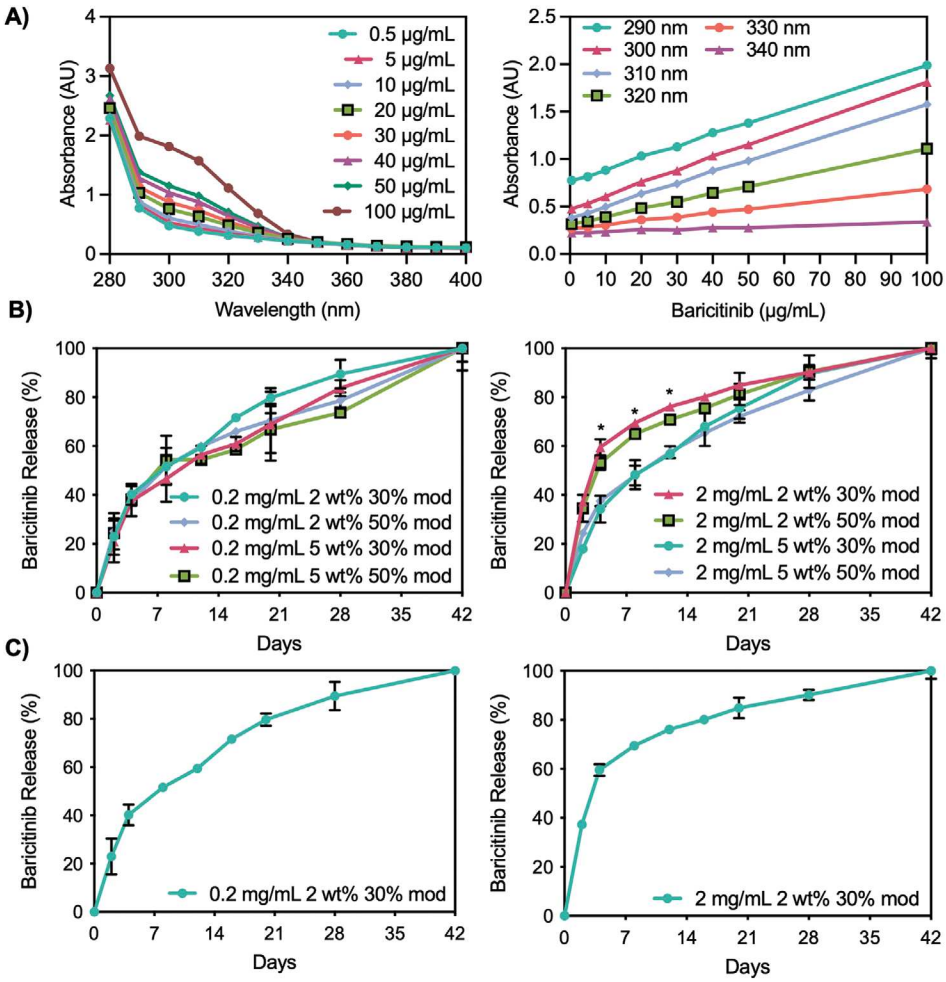

Figure 6. Baricitinib release and ultraviolet spectrometry. A) Quantification of baricitinib aromatic absorption in ultraviolet A and B range (280-400 nm) demonstrating highest absorption in the ultraviolet B range. Subsequent plotting of absorbance against dose demonstrates linear absorption at 300 nm leads to linear equation ($y = 0.01344x + 0.4769$, $R^2 = 0.9992$). B) Measuring baricitinib release at 300 nm against a standard curve allows quantification of baricitinib release from hydrogel formulations. Tunable release is exhibited over the course of six weeks with release dependent on material formulation. *$p<0.05$ between groups at each timepoint, $n = 3$ per timepoint, mean ± SD. C) Release curves for hydrogels assembled at 0.2 mg mL^{-1} or 2 mg mL^{-1} baricitinib loaded (2 wt.% hydrogel, 30% thiol modification).

3. Conclusion

Here, we engineered an injectable hydrogel that sustains the release of baricitinib through reversible thioimidate chemistry. Thiolated hyaluronic acid supported the formation of thioimidates between baricitinib and thiols as well as disulfide crosslinking for hydrogel formation. In hydrogels, baricitinib was released over six weeks and was active in inhibiting JAK-STAT signaling in vitro and in vivo in a mouse model of psoriasis. Further, this platform can be utilized with other JAK inhibitors containing nitrile groups (e.g., ruxolitinib, tofacitinib) in other inflammatory skin disorders that converge on JAK-STAT signaling such as atopic dermatitis, alopecia areata, and hidradenitis suppurativa. These data support the use of hydrogels for delivery of small molecules locally to the skin to avoid systemic toxicity from oral administration.

This technology has high translational potential to the dermatology clinic where injections are routinely performed for various inflammatory skin diseases. We expect that hydrogels can be stored lyophilized to be reconstituted, or frozen to be thawed at the point-of-care in dermatology clinics. Patients requiring treatment would have injections of hydrogels every few months into affected areas, which we expect to lead disease remission while preventing the off-target effects of systemic inhibition of the JAK-STAT pathway.

Further studies are needed to understand the pharmacokinetics of the baricitinib hydrogel and duration of efficacy in vivo in small animal models before pursuit of safety and efficacy in large animal models, and then human studies through clinical trials. Other relevant barriers to translation include adherence to good manufacturing practice (GMP), structural characterization after modification (identity, purity, potency), and evaluation of weight and polydispersity. Determination of sterilization, stability, handling, packaging, and storage is necessary prior to commercialization.[58] The current approval and ubiquitous use of hyaluronic acid hydrogels as dermal fillers in the skin will be

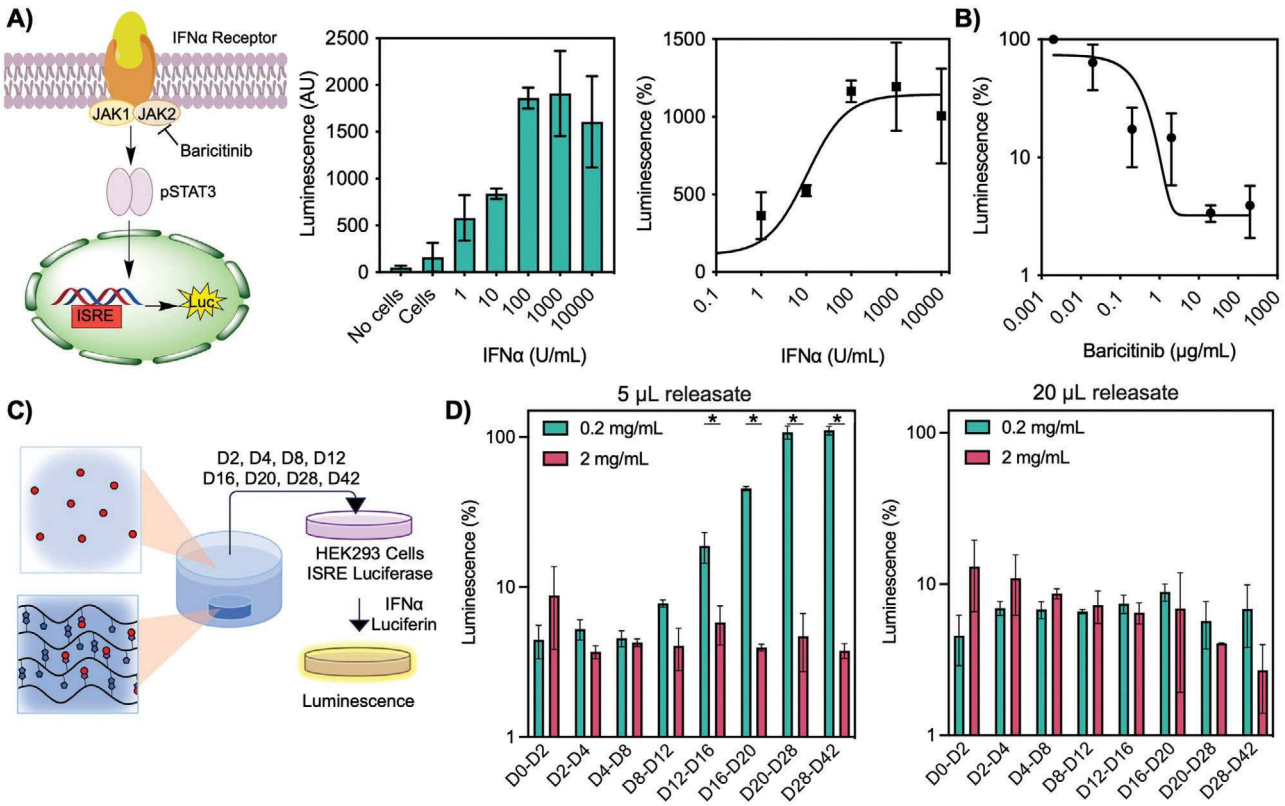

Figure 7. Validation of baricitinib activity on JAK/STAT signaling using a HEK293 luciferase reporter. A) HEK293 cell line with the firefly luciferase gene under the control of Interferon Stimulated Response Element (ISRE) where type I interferon-induced JAK/STAT signaling pathway in the target cells can be monitored by measuring luciferase activity. IFNα (EC_{50} = 15 U mL^{-1}) leads to induction of luminescence, n = 3 per group, mean ± SD. B) After stimulation with 100 U mL^{-1} IFNα, baricitinib leads to near complete silencing of luciferase activity, n = 3 per group, mean ± SD. C) Schematic of experimental design demonstrating hydrogel incubation in saline with collection and replacement of releasate performed at regular intervals and then added directly to cells. D) Incubation of cells with 5 μL releasates demonstrates sustained JAK/STAT inhibition but only from the 2 mg mL^{-1} formulation, n = 3 per group, mean ± SD, *p<0.05 between 0.2 mg mL^{-1} and 2 mg mL^{-1}. Incubation of cells with 20 μL of releasates demonstrates near complete inhibition of JAK/STAT signaling at all tested timepoints, n = 3 per group, mean ± SD. Luminescence is normalized to signals from cells with IFNα.

an advantage for translation of this material, although the inclusion of a biologically active JAK inhibitor will require approval as a drug rather than a medical device from the US FDA.

4. Experimental Section

4.0.0.1. Materials: Thiolated hyaluronic acid was purchased from a supplier (HAworks, Bedminster, NJ), synthesized as previously described through an amidation reaction at the carboxyl of hyaluronic acid with 30% or 50% degree of modification of disaccharides.[59] Polymers were stored under vacuum in a desiccator at room temperature. All other chemical reagents were purchased from Sigma-Aldrich (St. Louis, MO) and stored according to manufacturer's instructions unless otherwise indicated. All experiments were performed in triplicate unless otherwise indicated.

Liquid Chromatography-Mass Spectrometry (LCMS): Samples were prepared by mixing 500 μM of baricitinib with cysteamine, L-cysteine, or levamisole in distilled water. Samples were filtered through a 0.2 μm syringe filter before use. Nominal mass accuracy LCMS data were obtained using a Waters Acquity ultra-performance liquid chromatography (UPLC) system equipped with a Waters TUV detector (254 nm) and a Waters SQD single quadrupole mass analyzer with electrospray ionization. LC gradient 500 μL min^{-1}: 30 s hold 95:5 (water:acetonitrile 0.1% v/v formic acid), 2 min gradient to 5:95, and 30 s hold with Acquity UPLC high strength silica C18, 1.7 μm, 2.1×50 mm column.

Nuclear Magnetic Resonance (NMR): Samples were prepared by mixing 1 mg of baricitinib or thiolated hyaluronic acid in 400 μL D_2O. Samples were centrifuged to remove insoluble fractions prior to use. ^{1}H and ^{13}C spectra were recorded at 500.20 MHz and 125.78 MHz on a Bruker AVIII 500 MHz NMR spectrometer equipped with a Bruker 5 mm DCH Helium Cryoprobe. ^{1}H spectra of hyaluronic acid and baricitinib-hyaluronic acid were obtained in 32 K data points over 8 kHz spectral width using the water suppression pulse program, noesygppr1d, to suppress the water peak. ^{1}H spectrum of baricitinib was obtained in 64K data points over 10 kHz spectral width using a 30° flip-angle pulse. ^{13}C spectra were obtained in 64K data points over 29.761 kHz spectral width using the pulse program, zgpgsezr, a z-restored spin-echo ^{13}C pulse sequence with power-gated ^{1}H decoupling. A 2s relaxation delay was used between acquisitions. The free induction decays were processed using exponential window function (line-broadening 0.3 Hz for ^{1}H and 1 Hz for ^{13}C) before Fourier transformation.

Thiol Quantification Assays: The Free Thiol Assay Kit (ab112158, Abcam, Waltham, MA) was used for all thiol quantification measurements. Solutions of thiolated hyaluronic acid in distilled water were mixed with a solution of baricitinib in 1:1 dimethyl sulfoxide (DMSO) to distilled water to the indicated final concentrations in 100 μL total volume including 50 μL of assay reaction mixture.[60] Solutions prior to addition of reaction mixture were gently vortexed and products were allowed to form for 20 min. After mixing, 50 μL of product was transferred to a black walled 96-well plate and products were incubated with 50 μL of the assay reaction

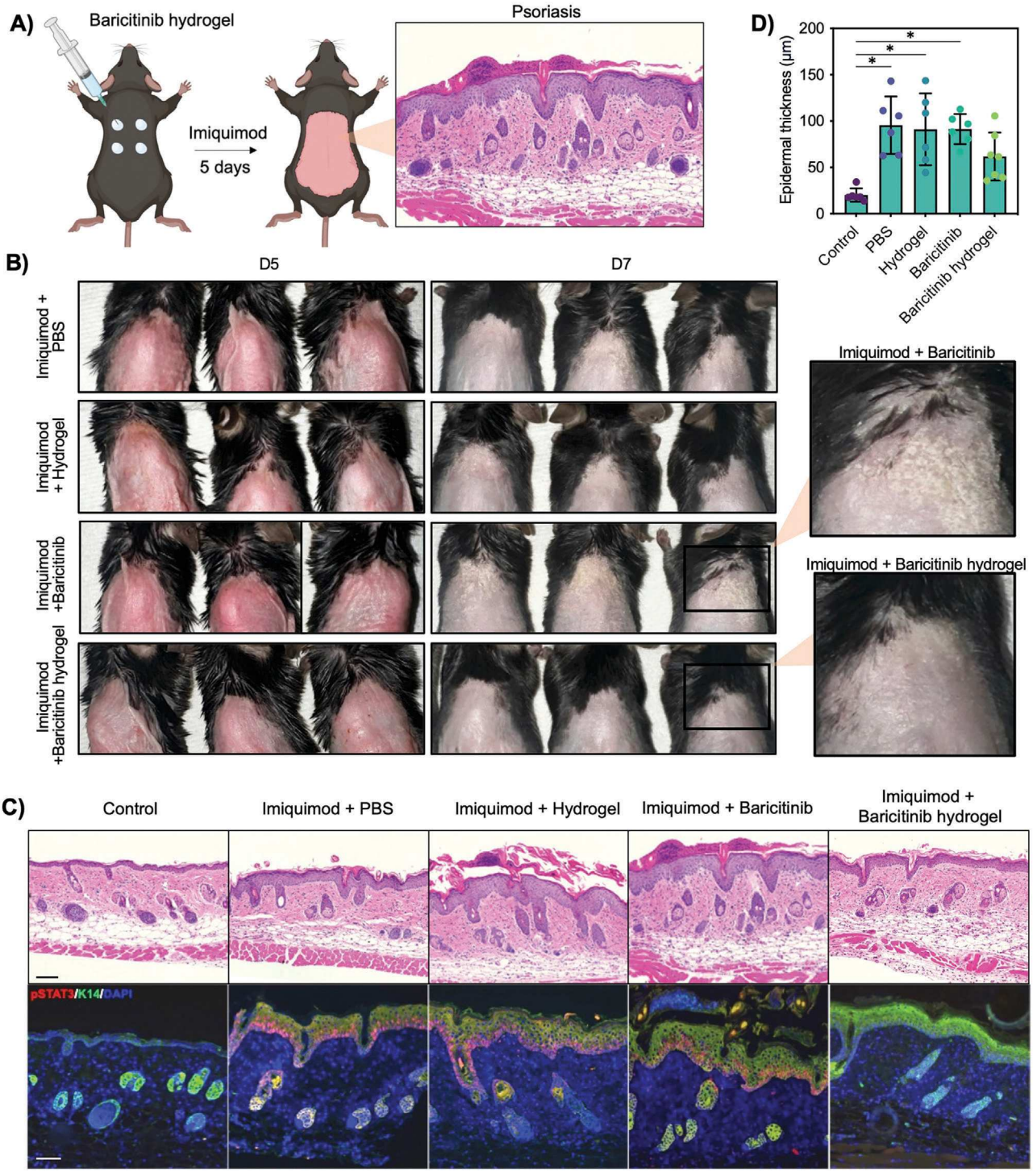

Figure 8. In vivo injections of baricitinib hydrogel in an imiquimod model of psoriasiform dermatitis. A) Two 25 uL injections of baricitinib hydrogel or PBS, hydrogel alone, or baricitinib alone controls are injected into four spots in dorsal mouse skin. After injection, imiquimod is applied daily for five days to induce psoriasiform inflammation before sacrifice. B) Images of skin changes at five days and seven days. C) H&E sections and pSTAT3 demonstrating skin thickening and pSTAT3 nuclear expression in response to imiquimod application with reduced thickening and pSTAT3 expression seen in treatment groups. Scale = 100 μm. Epidermal keratinocytes are counterstained with keratin 14 (K14) to highlight the hyperplastic epidermis. D) Quantification of epidermal thickness at seven days by quantifying epidermal ROI divided by length. *$p<0.05$ by one-way ANOVA, n = 6 for PBS, hydrogel, and baricitinib hydrogel groups, n = 5 for control and baricitinib groups, mean ± SD.

mixture according to manufacturer's protocols. Analyses were performed using the Biotek Synergy H1 microplate reader (ex/em: 490/520 nm).

Hydrogel Formation and in vitro Release: Hydrogels were formed by evenly mixing stock solutions of thiolated hyaluronic acid in phosphate-buffered saline (PBS) with stock solutions of baricitinib in DMSO to the final desired weight percent concentration (w/v) and allowed to mix and crosslink for 24 h.[60] After 24 h, hydrogels were centrifuged and DMSO was removed by briefly washing hydrogels in 1 mL PBS (3×5 min). For release studies, 100 µL of hydrogel was incubated in 200 µL of PBS at room temperature and releasates were collected and replaced with fresh PBS at days 2, 4, 8, 12, 16, 20, 28, and 42. At the final timepoint, hydrogels were manually disrupted. Absorbances were measured at 300 nm the Biotek Synergy H1 microplate reader and baricitinib concentrations were determined from a standard curve and summed to obtain cumulative release. For in vivo studies, hydrogels were prepared under sterile conditions, transferred to a 27G x ½″ syringe (Becton Dickinson, Franklin Lakes, NJ), and subsequently irradiated under ultraviolet light in accordance with prior reports.[10,11,61–63]

Shear Oscillatory Rheometry: Hydrogels were formed as described and deposited on the bottom plate of an HR 20 (TA Instruments, New Castle, DE) rheometer immediately after mixing or after 24 h of gelation. The rheometer was fitted with a 20 mm diameter stainless steel parallel plate geometry and placed at a 350 µm gap. Oscillatory rheological time sweeps (1% strain, 10 Hz) were performed to obtain the average storage (G′) and loss (G″) moduli, and oscillatory frequency sweeps (1% strain, 0.1 Hz to 100 Hz,) were obtained to characterize dynamic viscoelastic properties at both 25 and 37 °C.

Instron Mechanical Testing: Hydrogels were assembled in 27G x ½″ syringes and tested on an Instron 5564 Tabletop Universal Testing Machine using a 2 kN load cell at a displacement rate of 50 mm/min. Maximum required for extrusion were determined during the linear portion of the force-displacement curve.

HEK 293 Culture: Cells (BPS Bioscience, San Diego, CA) were thawed in Dulbecco's Modified Eagle Medium (DMEM) supplemented with 10% fetal bovine serum (FBS) and 1% penicillin/streptomycin. In subsequent studies, media was supplemented with 400 µg mL^{-1} of geneticin. Prior to use, cells were split into 96 well black-walled, clear bottom plates (300 000/well) in media without geneticin 24 h prior.

Luciferase Assays: For the interferon (IFNα) titration, varying concentrations from 10^{-1} to 10^{4} U/mL of IFNα at 100 µL total volume were incubated for 6 h. For the baricitinib condition, concentrations of 10^{-3} to 10^{3} µg mL^{-1} baricitinib were added to wells and incubated for 1 h. IFNα was added to each well at a final concentration of 100 U mL^{-1} at 100 µL total per well and incubated for 6 h. For the releasate assay, releasate volumes of 5 µL or 20 µL were added to cells in triplicate from each timepoint and incubated for 1 h. IFNα volume was added to a total of 100 µL and 100 U mL^{-1} and then incubated for 6 h. After the 6-h incubation of IFNα, luciferase activity was quantified for each of the three tests using the ONE-Step Luciferase Assay System (BPS Bioscience, San Diego, CA) with 100 µL master mix added for a total volume of 200 µL. The 96 well plate was placed on an orbital shaker for 15 min covered from light before taking luminescence measurements using the Biotek Synergy H1 microplate reader.

HaCAT Culture and Proliferation Assay: HaCaT cells were cultured in calcium-free DMEM with 10% FBS, and 1% penicillin/streptomycin. Cells were split into 24-well plates 24 h at 100 000/well. After 24 h, hydrogels were formed and 50 µL was transferred to a polycarbonate membrane transwell insert with 6.5 mm diameter, 0.1 µm pore size (Corning, Corning, NY) and coincubated with cells for the indicated times. The CellTiter 96 AQueous One Solution Cell Proliferation MTS Assay (Promega, Madison, WI) was utilized according to manufacturer's protocols. Absorbance was measured at 490 nm using the Biotek Synergy H1 microplate reader.

In vivo Studies and Tissue Processing: C57BL/6 female mice were used for imiquimod assays. After chemical epilation, hydrogels were injected into four sites intradermally into dorsal mouse skin. Imiquimod 5% cream was subsequently applied daily for five days before sacrifice at seven days. Standard histologic protocols using 4% paraformaldehyde and paraffin-embedding were utilized. Investigators were blinded through the histology process and imaging process. Images were analyzed using a Leica Microsystems DM6 B microscope equipped with a DFC9000 Camera or Keyence imaging system. At least two injection sites and four sections were stained with hematoxylin and eosin per mouse. Quantification of epidermal thickness was performed on stitched 10x slides of 6–10 mm skin sections by selecting the entire region-of-interest (ROI) of the epidermis using the Wand Tool on FIJI on Legacy Mode. The smooth feature was utilized to ensure the ROI appropriate captured the entire region between the granular layer and basal layer. The ROI area was measured and subsequently divided by the length of epidermis. Average epidermal thickness was obtained for two sections per mouse. For immunofluorescence, sections were processed according to standard protocols and stained with anti-pSTAT3 antibody (1:100, Cat No. 9145, Cell Signaling Technologies, Danvers, MA) and anti-cytokeratin 14 antibody (1:1000, Cat No. 906 001, BioLegend, San Diego, CA) overnight at 4 °C followed by incubation with secondary antibodies. All animal procedures were performed in accordance with the Institutional Animal Care and Use Committee at the University of Pennsylvania.

Statistics: All data were reported as mean ± standard deviation. Comparisons were performed between groups using Student's t-test or one-way ANOVA with post hoc testing. Bonferroni correction was used to account for multiple comparisons with $\alpha = 0.05$. All statistical analyses were performed in Graphpad Prism 9.

Supporting Information

Supporting Information is available from the Wiley Online Library or from the author.

Acknowledgements

The authors thank Dr. Matthew Davidson and Dr. Diana Kim for assistance in review of this manuscript, and David Polefrone for assistance with LCMS experiments, and Elaine Kim for assistance with immunofluorescence. The authors thank Dr. Charles W. Ross III, Director of Automated Synthesis and Characterization of Penn Chemistry and Mr. Ryan Kubanoff, BCRC Lab Manager, for providing chromatographic and mass spectral method development, training, analyses, and data interpretation. The authors thank Dr. Jun Gu, Director of NMR Facility of Penn Chemistry, for assistance with ^{1}H NMR and ^{13}C NMR data acquisition, analysis, and interpretation. The authors also thank Dr. Stephen Prouty from the Skin Biology and Diseases Resource-based Center for assistance with histology. The authors gratefully acknowledge the use of facilities and instrumentation (Instron 5564 Tabletop Universal Testing Machine) supported by the Department of Materials Science and Engineering Departmental Laboratory at the University of Pennsylvania. **Funding**: Support for this work was provided by the Penn Skin Biology and Diseases Resource-based Center, funded through a Pilot & Feasibility Grant (NIH/NIAMS grant P30-AR069589), the Edwin & Fannie Gray Hall Center for Human Appearances Research Grant, and the Qiu Family Dermatology Research Fund for support of research in the Department of Dermatology at the University of Pennsylvania. Mechanical testing is supported by the National Science Foundation (NSF) through the University of Pennsylvania Materials Research Science and Engineering Center (DMR-1720530).

Conflict of Interest

The authors declare no conflict of interest.

Data Availability Statement

The data that support the findings of this study are available from the corresponding author upon reasonable request.

Keywords

dermatology, hydrogel, JAK-STAT, psoriasis, thioimidate

Received: September 25, 2023
Revised: November 30, 2023
Published online:

[1] W. Damsky, B. A. King, *J. Am. Acad. Dermatol.* **2017**, *76*, 736.
[2] S. A. Hasni, S. Gupta, M. Davis, E. Poncio, Y. Temesgen-Oyelakin, P. M. Carlucci, X. Wang, M. Naqi, M. P. Playford, R. R. Goel, X. Li, A. J. Biehl, I. Ochoa-Navas, Z. Manna, Y. Shi, D. Thomas, J. Chen, A. Biancotto, R. Apps, F. Cheung, Y. Kotliarov, A. L. Babyak, H. Zhou, R. Shi, K. Stagliano, W. L. Tsai, L. Vian, N. Gazaniga, V. Giudice, S. Lu, et al., *Nat. Commun.* **2021**, *12*, 3391.
[3] A. Karatas, B. Oz, C. Celik, Z. A. Akar, R. F. Akkoc, E. O. Etem, A. F. Dagli, S. S. Koca, *Sci. Rep.* **2022**, *12*, 2553.
[4] E. Kozera, A. Flora, J. W. Frew, *J. Am. Acad. Dermatol.* **2022**, *87*, 1440 .
[5] F. Enjalbert, P. Dewan, M. P. Caley, E. M. Jones, M. A. Morse, D. P. Kelsell, A. J. Enright, E. A. O'toole, *J. Clin. Invest.* **2020**, *130*, 4798.
[6] S. R. Ytterberg, D. L. Bhatt, T. R. Mikuls, G. G. Koch, R. Fleischmann, J. L. Rivas, R. Germino, S. Menon, Y. Sun, C. Wang, A. B. Shapiro, K. S. Kanik, C. A. Connell, *N. Engl. J. Med.* **2022**, *386*, 316 .
[7] L. Hoisnard, B. Lebrun-Vignes, S. Maury, M. Mahevas, K. El Karoui, L. Roy, A. Zarour, M. Michel, J. L. Cohen, A. Amiot, P. Claudepierre, P. Wolkenstein, P. Grimbert, E. Sbidian, *Sci. Rep.* **2022**, *12*, 7140.
[8] J. Li, D. J. Mooney, *Nat. Rev. Mater.* **2016**, *1*, 16071.
[9] E. Caló, V. V. Khutoryanskiy, *Eur. Polym. J.* **2015**, *65*, 252.
[10] L. L. Wang, J. J. Chung, E. C. Li, S. Uman, P. Atluri, J. A. Burdick, *J Controlled Release* **2018**, *285*, 152.
[11] L. L. Wang, Y. Liu, J. J. Chung, T. Wang, A. C. Gaffey, M. Lu, C. A. Cavanaugh, S. Zhou, R. Kanade, P. Atluri, E. E. Morrisey, J. A. Burdick, *Nat. Biomed. Eng.* **2017**, *1*, 983.
[12] S. Jindal, R. Awasthi, K. Goyal, G. T. Kulkarni, *Dermatol. Ther.* **2022**, *35*, e15830.
[13] A. Mandal, J. R. Clegg, A. C. Anselmo, S. Mitragotri, *Bioeng. Transl. Med.* **2020**, *5*, e10158.
[14] J. E. Mealy, C. B. Rodell, J. A. Burdick, *J. Mater. Chem. B* **2015**, *3*, 8010.
[15] X.-Q. Zheng, J.-F. Huang, J.-L. Lin, Y.-X. Zhu, M.-Q. Wang, M.-L. Guo, X.-J. Zan, A.-M. Wu, *Colloids Surf., B* **2021**, *199*, 111532.
[16] A. I. Baraian, et al., *Polymers (Basel)* **2023**, *15*, PMC9962605.
[17] R. T. Malatani, S. Bilal, A. Mahmood, R. M. Sarfraz, N. Zafar, H. Ijaz, U. Rehman, S. Akbar, H. M. Alkhalidi, H. A. Gad, *Gels* **2023**, *9*, 187.
[18] J. Liang, Y. Yu, C. Li, Q. Li, P. Chen, W. Li, W. Liu, Z. Li, Y. Liu, S. Zhang, X. Zhang, *Carbohydr. Polym.* **2023**, *305*, 120549.
[19] H. K. Noddeland, M. Lind, L. B. Jensen, K. Petersson, T. Skak-Nielsen, F. H. Larsen, M. Malmsten, A. Heinz, *Acta Biomater.* **2023**, *157*, 149.
[20] A. Berteotti, F. Vacondio, A. Lodola, M. Bassi, C. Silva, M. Mor, A. Cavalli, *ACS Med. Chem. Lett.* **2014**, *5*, 501.
[21] S. Brogi, R. Ibba, S. Rossi, S. Butini, V. Calderone, S. Gemma, G. Campiani, *Molecules* **2022**, *27*, 2561.
[22] J. R. Brisson, P. R. Carey, A. C. Storer, *J. Biol. Chem.* **1986**, *261*, 9087.
[23] J. B. Moon, R. S. Coleman, R. P. Hanzlik, *J. Am. Chem. Soc.* **1986**, *108*, 1350.
[24] F. F. Fleming, L. Yao, P. C. Ravikumar, L. Funk, B. C. Shook, *J. Med. Chem.* **2010**, *53*, 7902.
[25] K. Mizuno, K. Takeuchi, K. Umehara, M. Nakajima, *Biochem. Pharmacol.* **2018**, *156*, 312.
[26] D. R. Owen, C. M. N. Allerton, A. S. Anderson, L. Aschenbrenner, M. Avery, S. Berritt, B. Boras, R. D. Cardin, A. Carlo, K. J. Coffman, A. Dantonio, L. Di, H. Eng, R. Ferre, K. S. Gajiwala, S. A. Gibson, S. E. Greasley, B. L. Hurst, E. P. Kadar, A. S. Kalgutkar, J. C. Lee, J. Lee, W. Liu, S. W. Mason, S. Noell, J. J. Novak, R. S. Obach, K. Ogilvie, N. C. Patel, M. Pettersson, et al., *Science* **2021**, *374*, 1586.
[27] B. Korkmaz, A. Lesner, S. Marchand-Adam, C. Moss, D. E. Jenne, *J. Med. Chem.* **2020**, *63*, 13258.
[28] S. Krishnan, R. M. Miller, B. Tian, R. D. Mullins, M. P. Jacobson, J. Taunton, *J. Am. Chem. Soc.* **2014**, *136*, 12624.
[29] R. M. Oballa, et al., *Bioorg. Med. Chem. Lett.* **2007**, *17*, 998.
[30] P. A. MacFaul, A. D. Morley, J. J. Crawford, *Bioorg. Med. Chem. Lett.* **2009**, *19*, 1136.
[31] M. Forster, A. Chaikuad, S. M. Bauer, J. Holstein, M. B. Robers, C. R. Corona, M. Gehringer, E. Pfaffenrot, K. Ghoreschi, S. Knapp, S. A. Laufer, *Cell Chem. Biol.* **2016**, *23*, 1335.
[32] J. Kempson, D. Ovalle, J. Guo, S. T. Wrobleski, S. Lin, S. H. Spergel, J. J.-W. Duan, B. Jiang, Z. Lu, J. Das, B. V. Yang, J. Hynes, H. Wu, J. Tokarski, J. S. Sack, J. Khan, G. Schieven, Y. Blatt, C. Chaudhry, L. M. Salter-Cid, A. Fura, J. C. Barrish, P. H. Carter, W. J. Pitts, *Bioorg. Med. Chem. Lett.* **2017**, *27*, 4622.
[33] J. A. Burdick, G. D. Prestwich, *Adv. Mater.* **2011**, *23*, H41.
[34] X. Li, A. Sigen, Q. Xu, F. Alshehri, M. Zeng, D. Zhou, J. Li, G. Zhou, W. Wang, *ACS Appl. Bio. Mater.* **2020**, *3*, 4756.
[35] Y. Qing, et al., *Angew Chem Int Ed Engl* **2020**, *59*, 15711.
[36] S.-B. Yong, H. J. Kim, J. K. Kim, J. Y. Chung, Y.-H. Kim, *Sci. Rep.* **2017**, *7*, 42171.
[37] T. Xie, et al., *Sci. Rep.* **2020**, *10*, 2476.
[38] F. C. Schaefer, G. A. Peters, *J. Org. Chem.* **1961**, *26*, 412.
[39] M. H. Chen, L. L. Wang, J. J. Chung, Y.-H. Kim, P. Atluri, J. A. Burdick, *ACS Biomater. Sci. Eng.* **2017**, *3*, 3146.
[40] B. G. Kapoor, S. V. Gandhi, *J. Drug Delivery Ther.* **2019**, *9*, 488.
[41] R. Mohammadi-Meyabadi, N. Beirampour, N. Garrós, H. L. Alvarado, D. Limón, M. Silva-Abreu, A. C. Calpena, M. Mallandrich, *Pharmaceutics* **2022**, *14*, 2714.
[42] A. I. Neto, et al., *Small* **2014**, *10*, 2459.
[43] N. C. Pan, H. C. B. Pereira, M. D. L. C. Da Silva, A. F. D. Vasconcelos, M. A. P. C. Celligoi, *Appl. Biochem. Biotechnol.* **2017**, *182*, 276.
[44] J. Hafsa, M. A. Chaouch, B. Charfeddine, C. Rihouey, K. Limem, D. Le Cerf, S. Rouatbi, H. Majdoub, *Pharm. Biol.* **2017**, *55*, 156.
[45] D. Hebenstreit, J. Horejs-Hoeck, A. Duschl, *Drug News Perspect* **2005**, *18*, 243.
[46] L. Pedranzini, T. Dechow, M. Berishaj, R. Comenzo, P. Zhou, J. Azare, W. Bornmann, J. Bromberg, *Cancer Res.* **2006**, *66*, 9714 .
[47] L. Van Der Fits, S. Mourits, J. S. A. Voerman, M. Kant, L. Boon, J. D. Laman, F. Cornelissen, A.-M. Mus, E. Florencia, E. P. Prens, E. Lubberts, *J. Immunol.* **2009**, *182*, 5836.
[48] M. Jabeen, A.-S. Boisgard, A. Danoy, N. El Kholti, J.-P. Salvi, R. Boulieu, B. Fromy, B. Verrier, M. Lamrayah, *Pharmaceutics* **2020**, *12*, 789.
[49] K. A. Papp, M. A. Menter, M. Raman, D. Disch, D. E. Schlichting, C. Gaich, W. Macias, X. Zhang, J. M. Janes, *Br. J. Dermatol.* **2016**, *174*, 1266 .
[50] H. B. Deepak, S. E. Prince, P. Deshpande, *Indian J Pharmacol* **2022**, *54*, 183.
[51] A. C. Gaffey, M. H. Chen, C. M. Venkataraman, A. Trubelja, C. B. Rodell, P. V. Dinh, G. Hung, J. W. Macarthur, R. V. Soopan, J. A. Burdick, P. Atluri, *J. Thorac. Cardiovasc. Surg.* **2015**, *150*, 1268.
[52] X. Z. Shu, Y. Liu, F. Palumbo, G. D. Prestwich, *Biomaterials* **2003**, *24*, 3825.
[53] H. Lee, T. W. Lee, A. Chandrasekharan, S.-E. Sung, S.-G. Yim, S. Kim, K.-Y. Seong, M.-S. Seo, S. Y. Yang, *ACS Biomater. Sci. Eng.* **2022**, *8*, 1613.
[54] S. Bian, M. He, J. Sui, H. Cai, Y. Sun, J. Liang, Y. Fan, X. Zhang, *Colloids Surf., B* **2016**, *140*, 392.
[55] S. K. Hahn, J. K. Park, T. Tomimatsu, T. Shimoboji, *Int. J. Biol. Macromol.* **2007**, *40*, 374.

[56] M. Master, S. Roberts, *Plast. Reconstr. Surg. Glob. Open* **2022**, *10*, e4252.
[57] K. Y. Park, J. Seok, B. J. Kim, C. S. Youn, *Dermatol. Surg.* **2017**, *43*, 1306.
[58] G. Huerta-Ángeles, K. Nesporová, G. Ambrozová, L. Kubala, V. Velebný, *Front. Bioeng. Biotechnol.* **2018**, *6*, 62.
[59] A. Díaz, H. Herrada-Manchón, J. Nunes, A. Lopez, N. Díaz, H.-J. Grande, I. Loinaz, M. A. Fernández, D. Dupin, *Macromol. Rapid Commun.* **2022**, *43*, 2200449.
[60] S. M Alshahrani, F. Shakeel, *Molecules* **2020**, *25*, 2124.
[61] L. L. Wang, J. N. Sloand, A. C. Gaffey, C. M. Venkataraman, Z. Wang, A. Trubelja, D. A. Hammer, P. Atluri, J. A. Burdick, *Biomacromolecules* **2017**, *18*, 77.
[62] C. B. Rodell, J. W. Macarthur, S. M. Dorsey, R. J. Wade, L. L. Wang, Y. J. Woo, J. A. Burdick, *Adv. Funct. Mater.* **2015**, *25*, 636.
[63] S. Uman, L. L. Wang, S. L. Thorn, Z. Liu, J. S. Duncan, A. J. Sinusas, J. A. Burdick, *Adv. Healthcare Mater.* **2020**, *9*, 2000294.